RESEARCH

A numerical investigation study on tunable graphene-squared pixel array-based infrared polarizer

Fahad Ahmed Alzahrani[1] · Vishal Sorathiya[2]

Abstract

This paper proposes a tunable graphene-silica-assisted squared pixel array-shaped polarizer construction for the infrared frequency range. A silica and pixel graphene array layered structure was used to create the tunable polarizer. The polarizer behavior of the structure is studied over the 1–15 THz of infrared frequency. Single-layer graphene sheet Fermi energy/chemical potential is adjustable for the proposed structure. The transmittance coefficient and phase variation response are presented for the different pixel array modes of the designs. The overall behavior of the structure is evaluated in terms of the co- and cross-polarization effect. The behavior of the phase difference, polarization conversion rate, and wide-angle stability are presented for two of the overall pixel array structures. The proposed structure of the polarizer allows choosing the resonating conditions over 1–15 THz of the band using different pixel array geometries, transmittance and phase variation responses. Electro-optical structures in the lower THz band can benefit from the proposed results of this tunable polarizer structure.

1 Introduction

The term "metamaterial" refers to any substance created by an artificial process. Compared to the light modeling capabilities offered by standard planar interfaces, dimension-reduced metasurfaces have yielded significantly superior results [1], increasing interest in studying these surfaces. Components of the structure are placed in such a way that they produce dense and ultra-thin arrays in two dimensions (2-D). In addition, they possess unique qualities due to the nature that causes them to resonate [2]. As a result, producing metasurfaces is a straightforward process and does not require much room for more investigation. Furthermore, they have a unique feature in controlling microwave and optical frequencies [3]. Therefore, this meta-atom-based material has the potential to be used in the construction of different optical devices, such as lenses and holograms. Consequently, frequency selective surfaces, also known as FSSs, are utilized in radiophysics rather than optical metasurfaces, which are considered more contemporary creations [4–7].

Graphene's extraordinary qualities are being studied to the hilt, which only adds to its allure. The honeycomb lattice of a single atom forms the basis of this monolayer structure [8]. Low density makes it more temperature and chemical potential sensitive [9, 10] because of its structure. The frequency range of graphene's conductivity spans from the near-infrared to the very tiny THz range. The weak plasmonic resonance results from the low carrier concentration, which has sparked a great deal of curiosity among researchers [5, 11]. Metamaterials are substances created in a laboratory. Various properties, including petite sizes, low cost, and ultra-thin nature, make metamaterials a preferred choice for design and use. To get the negative hyperbolic dispersion [7], refractive index [12], and perfect lens [13], metamaterials must be designed and developed. The display of graphene's thermal, electrical, mechanical, and optical properties is determined by its honeycomb-shaped two-dimensional structure of monolayered carbon atoms. The two-dimensional graphene structure's tunability behavior is studied using Dirac fermions. Thermal tuning [14], optical pump [15], and chemical doping [16] can all be used to alter further and modify graphene's properties [17]. Graphene-based absorbers and other metamaterials, such as those with negative refractive index values, clocking, and imaging at

✉ Vishal Sorathiya
vishal.sorathiya9@gmail.com

Fahad Ahmed Alzahrani
Fayzahrani@uqu.edu.sa

1 Computer Engineering Department, Umm Al-Qura University, Mecca, Saudi Arabia

2 Faculty of Engineering and Technology, Parul Institute of Engineering and Technology, Parul University, Waghodia Road, Vadodara, Gujarat 391 760, India

subwavelength wavelengths, have also shown promising results. Optical polarisers and other polarization devices are required for optical communications systems and polarization-dependent optical sensors. To interface with fiber networks, we need to align and modify the bulk optical configurations of standard polarizers [18]. Because of graphene's inductive behavior in the THz band and its surface conductivity that may be influenced by biasing electrostatic or magnetostatic fields, small devices, passive components, and antennas made of graphene are now possible for THz applications [19]. Quality graphene is difficult to achieve in practical sizes for microwave device implementations due to its wavelength being considerably shorter than its huge surface area. The tide is turning, though. Commercially available CVD graphene sheets of high quality and big area are currently available [20]. The effective permittivity and permeability of synthetic metamaterials based on microwave frequency structures can be modified to obtain values much beyond those seen in nature, giving them significant electromagnetic wave manipulation capabilities [6, 21, 22]. Since surface reactance can be ignored in favor of surface resistance in the low-frequency region, absorbing materials are excellent in this frequency range. We are not aware of any studies that have been conducted to investigate the possibility of graphene functioning low loss FSR with conditions of omnidirectional resistor. To put it another way, flakes and nanoplates of graphene are much less expensive than monolayer graphene, which has significant resistance and is expensive to produce [23].

As a result of its low costs and ultra-thin thickness, graphene is well suited to numerous electrical and optical device applications [24]. When using metamaterials, we can generate optical properties that are not possible with traditional materials, such as hyperbolic dispersion, perfect lens, or a negative refraction index [13, 25–27]. Leaky-wave antennas [28], polarizers [25], and tunable absorbers [5, 29] are all examples of reconfigurable devices in which graphene is often utilized. The Dirac cone [30] can study graphene's intraband conductivity concept. Graphene has been shown to give the control action via an external electrostatic or electromagnetic field [31] that changes from material to material. Graphene's transition from the high terahertz [32] to the low terahertz [33] region has resulted in an increase in electrical and optical conductivity [37, 38]. Photonic systems based on graphene use single-layered sheets to create an integrated geometry. The various graphene sheet geometries [6, 34] can be used to investigate the principle of creating graphene polarization structures [35]. Periodically directed structures can be created using polarizers, which act as electromagnetic filters. Radiographic antennas, metamaterials, and other electromagnetic equipment can be utilized for various applications, including reducing radar cross-sections [36]. Externally adjustable frequency and chemical graphene

potentials are the primary tuning tools for polarizers based on graphene [37]. It is critical to determine the transmittance and reflectance of the graphene-assisted components for them to have a metamaterial effect. The degree of variability in an attribute can be altered by varying the physical parameters of a graphene-based device. It is also possible to overcome the problems of thickness and tunability [38] with graphene-based metasurfaces. Single-layered graphene sheets can be used to create metasurfaces on a variety of substrates, including gold [38], aluminum [39], and silica [6]. For example, a single graphene sheet can be used to create a variety of device forms, including *L* [40], *T* [41], *C* shapes [25] and rectangular split rings [42]. It may be challenging to fabricate this structure in the exact shape we want. DLP lithography-based devices and oxygen plasma-based sources [43] can be used to create simple graphene patch-based structures.

1.1 Pixel-based tunable polarizer

The pixel-based graphene-based tunable polarizer is designed to investigate over 1–15 THz of the frequency spectrum range. The pixel array-based graphene structure is formed on top of the silica substrate. The overall dimensions of the structure (*L*) are set as 7.6 μm. The height of the silica substrate is set as 1.5 μm. The pixel-shaped graphene engraved space dimension is set as $p = 1.5$ μm and $g = 0.5$ μm. The *X* and *Y* axes of the proposed polarizer is set as periodic boundary conditions. The wave is imparted from the top of the pixel-based polarizer structure, as shown in the three-dimensional view of Fig. 1. The reflectance and transmittance responses are observed to identify the amplitude variation and other responses.

The proposed structure is analyzed over eight different pixel configurations, as shown in the top view configuration of Fig. 1. The graphene-based structure can be realized by various simulation techniques, such as the finite-element method (FEM) and finite-difference time domain (FTTD) [44, 45]. A simulation of a wideband absorber based on a gold resonator is performed with the help of the finite-element method in order to acquire quantitative data. This simulation is carried out in order to FEM. The usage of partial differential equations, often known as PDEs, is a technique implemented to find solutions to problems that are influenced by both time and space. Because of the famously difficult nature of PDEs and geometries, analytical methods are notoriously unreliable when solving the great majority of these problems. Instead, the approximation is arrived at by utilizing several different approaches to solving equations to break them down into their parts of equations found within the framework of the numerical model. When partial differential equations (PDEs) are approximated with the assistance of numerical model equations, it is possible to

Fig. 1 Schematic of the tunable graphene pixel-based infrared polarizer. Three-dimensional view of the pixel-based polarizer structure with different eight-pixel (D1–D8) configurations (top view)
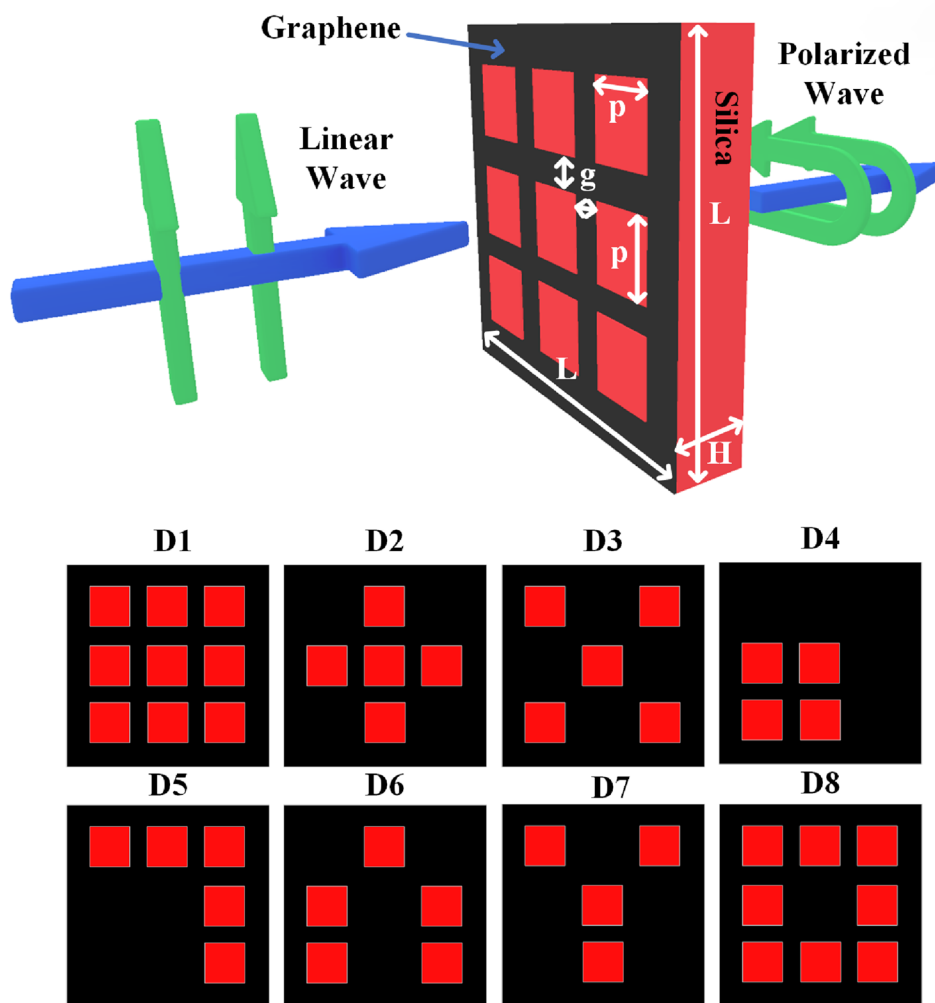
apply numerical techniques to solve them. It makes the use of numerical techniques a practical option. These numerical models can generate an estimate relatively near the actual response. The finite-element approach is one of the technologies utilized to determine precise equivalency (FEM). The fundamental equation for this FEM is shown in the following equation:

$$\nabla \times \mu_r^{-1}(\nabla \times \mathbf{E}) - k_0^2 \left(\epsilon_r - \frac{j\sigma}{\omega\epsilon_0}\right)\mathbf{E} = 0 \quad (1)$$

The Kubo formula [31] can be used to express the single-layered graphene conductivity equation. The intraband and interband terms can express the graphene conductivity equation. The surface current density can express the surface conductivity of the graphene with the equation $(J_x, J_y) = (E_x\sigma_s, E_y\sigma_s)$. The surface conductivity equation is defined in the following equation:

$$\sigma_s = \frac{-je^2 k_B T}{\pi\hbar^2(\omega - j2\Gamma)}\left(\frac{\mu_c}{k_B T} + 2\ln\left(e^{-\frac{\mu_c}{k_B T}} + 1\right)\right) \\ + \frac{-je^2}{4\pi\hbar}\ln\left(\frac{2|\mu_c| - (\omega - j2\Gamma)\hbar}{2|\mu_c| + (\omega - j2\Gamma)\hbar}\right) \quad (2)$$

In this equation, ω is defined as radian frequency which varies between 1 and 15 THz. $\hbar$ and k_B are defined as the reduced plank constant and Boltzmann constant. The value of the temperature (T), scattering rate (Γ) and electron relaxation time (τ^{-1}) is defined as 300 K, 10^{-11} and 10^{-13} s, respectively. The graphene chemical potential/Fermi energy value (μ_c) is varied between 0.1 and 0.9 eV. Chemical vapor deposition (CVD) [46], molecular beam epitaxy (MBE) [47], and cleavage procedures [48] are the most prevalent ways of generating graphene with single-layered geometry and other two-dimensional materials. It is possible to form nanomaterial structures using different methods such as nanolithography (Atomic Force technique) [49], structure printing of plasmonic devices [50], and the

Nano-Spheric Process [51]. The lithography techniques for non-spheric shapes [51] and nanoplasmonics devices [50] can be used to construct a complex structure on top of graphene. Lithography technologies have been used to create graphene composites with high-quality and adaptable complex nano- and micro-shapes, as demonstrated in [50]. The suggested structure can be manufactured without electron beam lithography methods and CVD. Providing a tuning mechanism for graphene-based polarizer structures can be possible by employing ion gel formation on structures produced by CVD and DLP laser lithography. This fabrication method forms graphene on copper foil via the CVD process. Copper can be removed from the graphene using an ammonium persulfate solution in a wet transfer technique [52, 53]. A pixel-based graphene sheet array can be created using an oxygen plasma at a specified power level [43]. DLP laser lithography can be used to create metal grids or patches on top of graphene. Ion gel of 1-ethyl-3-methylimidazolium bis(trifluoromethyl sulfonic) imide and polyvinylidene fluoride-cohexafluoropropylene can be used to tune the graphene for varied bias voltages [54, 55].

2 Results and discussion

This structure is investigated using the professional software package of COMSOL Multiphysics which offers the finite-element method of computation. It is seen in Fig. 2 that pixel array design 1 (D1) has a variance in reflectance and transmittance. This response is calculated for the multiple varieties of the graphene sheet chemical potential/Fermi energy values. As shown in Fig. 1 (a), the transmittance response can be tuned by altering the graphene chemical potential/Fermi energy. It can be seen in Fig. 2 that there is a similar variance in reflectance for the different values of chemical potential/Fermi energy (b). The transmittance coefficient for co-polarization is calculated using Eq. 3. While phase variation and phase difference between co-polarization and cross-polarization is calculated using Eqs. 4 and 5. Finally, the variation in the polarization conversion rate (PCR) is calculated using Eq. 6 for the co-polarized and cross-polarized reflectance coefficient:

$$T_{ij} = \left| E_j^{\text{Trans}} / E_i^{\text{Inc}} \right| (i, j = x, y),$$
$$\text{where} \quad E_j^{\text{Trans}} (j = x, y) \tag{3}$$

$$\Phi_{ij} = \arg \left(E_j^{\text{Trans}} / E_i^{\text{Inc}} \right) (i, j = x, y) \tag{4}$$

$$\Delta\Phi = \Phi_{xx} - \Phi_{yy} \tag{5}$$

$$\text{PCR} = \left| T_{xy} \right|^2 / \left[\left| T_{xx} \right|^2 + \left| T_{xy} \right|^2 \right] \tag{6}$$

This polarizer structure will allow the wave's passing to interact with the graphene layer. We have identified the effect and behavior of the polarizer by looking at its transmittance properties. The different dipole moments are created across the pixel array structure. The main effect of the polarization is caused by the energy concentration at the graphene edges created by the pixel geometry. These geometries will allow resonating at specific frequencies and potential chemical values. In Fig. 2, we can identify several resonating peaks at various frequencies and chemical potentials/Fermi energies. Figure 3 illustrates how each array configuration affects the resonance conditions. The graphene chemical potential/Fermi energy value of 0.9 eV is used to derive these transmittance responses. The resonating and transmittance peaks have a completely distinct influence on all pixel-based geometries. We have estimated a function that can be used to determine the structure's size and resonance frequency. The three functions of the relationship between L and f have been determined. Graphene's initial resonant
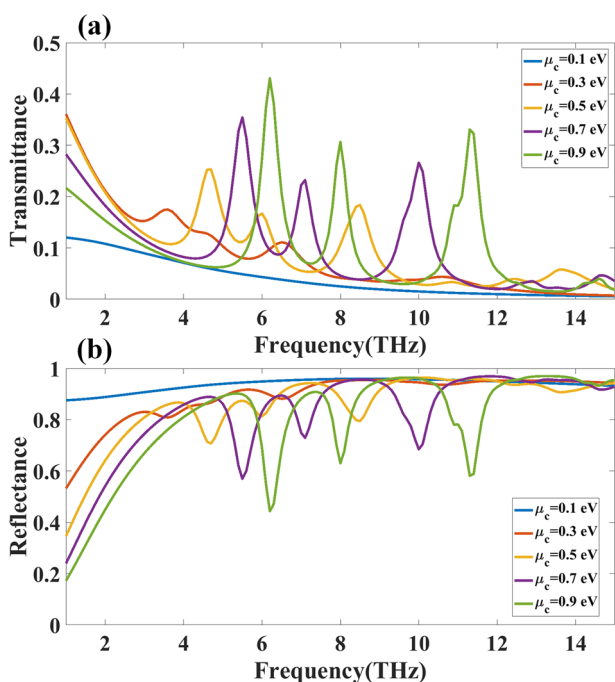

Fig. 2 a Calculated amplitude variation in transmittance for the pixel configuration D1 structure. **b** Calculated amplitude variation in reflectance for the pixel configuration D1 structure
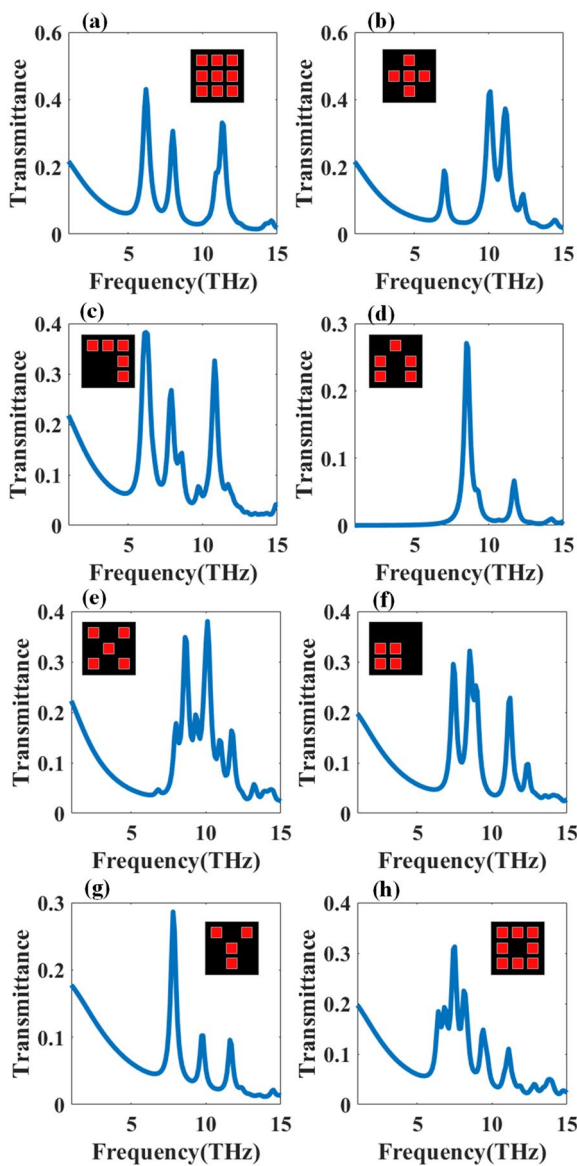
Fig. 3 Transmittance amplitude responses for various pixel configurations were calculated. The graphene sheet's chemical potential/Fermi energy is set to 0.9 eV for the duration of the experiment
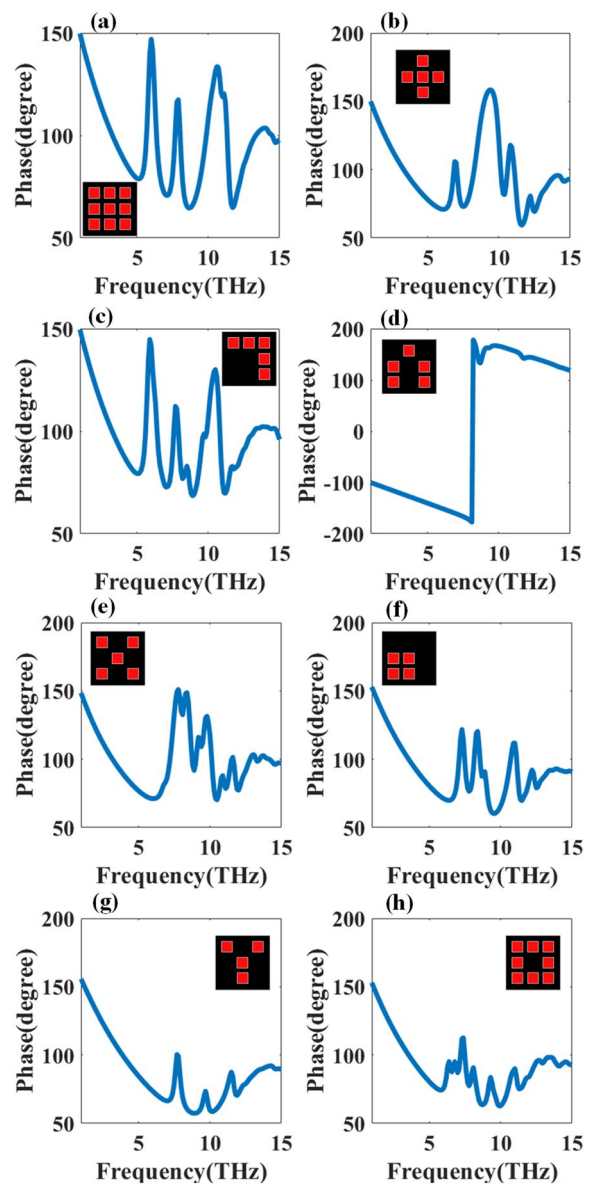

Fig. 4 Calculated transmittance phase (degree) response variation for the different pixel configurations. The chemical potential/Fermi energy of the graphene sheet is set as 0.9 eV for all the response

frequency is calculated using the structure's length and width in conjunction with its purpose. The equation used to identify the initial resonating frequency is $f_r \cong \sqrt{E_f/L}$ [56]. Furthermore, the pixel-based arrangement makes this single resonating frequency values to the multiple resonating conditions because individual pixel arrangement changes the overall resonance conditions. The proposed polariser structure's pixel arrangements presented the maximum possible geometries for the 3×3 pixel arrangements. The dipole moments generated through this pixel generation differ in all cases. Figure 3a, b, e, g is the mirrored geometries over X and Y directions which show a distinct resonance condition and transmittance effect over the simulated frequency

spectrum. In other cases of the pixel arrangement where the non-mirrored arrangement are shown, the resonance effect is different for all the pixel arrangement. This resonance effect in non-mirrored arrangement can be changed by rotating the same pixel arrangements. The resonance effect also depends on the pixel arrangement in line or scattered. Figure 4 shows the reflectance angle variation for the different design structures. We have set the Fermi energy/chemical potential number as 0.9 eV to get these results. In Designs (D1, D2, D3 and D8) structure, the overall geometry for the X direction and Y direction are identical, so the transmittance amplitude response $T_{xx} = T_{yy}$. In this context, the phased variation
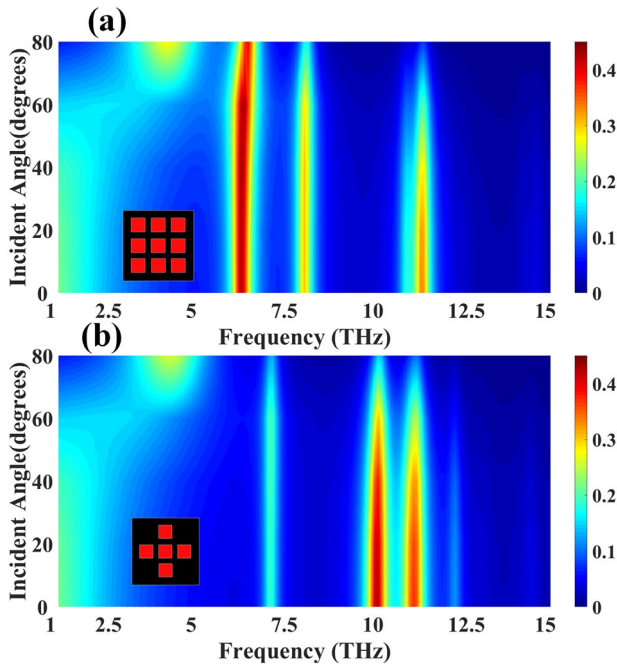
Fig. 5 Calculated variation in transmittance for pixel, **a** design 1, **b** design 2. The transmittance response is calculated for the different incident wave oblique incident angles ranging from 0° to 80°

shows the linear to liner polarization while phase change is observed between $-180°$ and $180°$. In the case of the designs (D4, D5, D6 and D7), the transmittance amplitude response $T_{xx} \neq T_{yy}$ and $\Delta\Phi = 90°$ or $T_{xx} = T_{yy}$ and $\Delta\Phi = 90°$

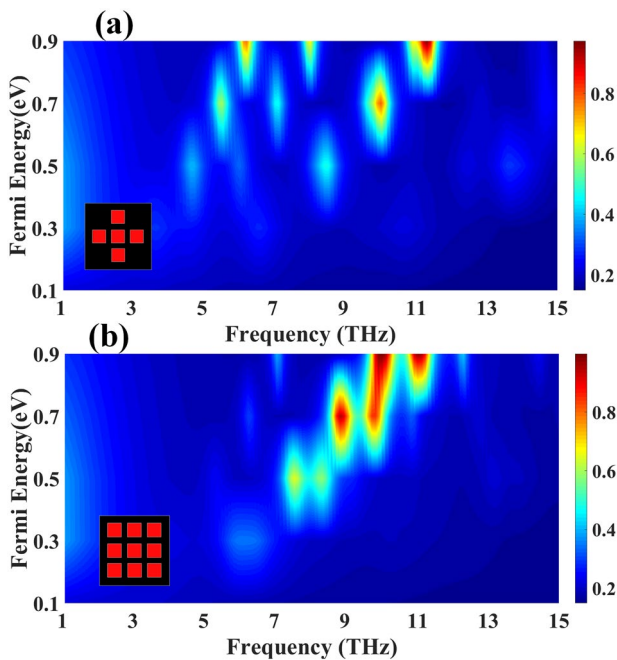generates the linear to circular or linear to elliptical polarizer conversion. We have calculated the transmittance response for the wide oblique incident angle with a range of 0°–80°. Figure 5a shows the variation in transmittance for design 1, and Fig. 5b shows the variation in transmittance for design 2 for the oblique incident angle. The maximum amplitude stability is observed up to 60° for design 1 and 80° for design 2. The stability in transmittance is also observed up to 60° of variation for > 7.5 THz frequency range. Figure 6a shows the variation in the PCR for the different values of graphene Fermi energy/chemical potential for design 1. Similarly, Fig. 6b shows the PCR variation for the different graphene Fermi energy/chemical potential values for design 2. It is observed the rise in PCR amplitude for the resonating condition for the multiple values of μ_c. We have also observed the variation in the phase difference for the relative PCR condition. The comparative plot of PCR and phase difference is shown in Fig. 7a, b for the design 1 and design 2 conditions. This response is generated for the 0.9 eV of graphene μ_c. It is observed that the value of the phase difference changes from $-200°$ to $200°$ allowing to choose the circular, linear and elliptical polarization for the different frequency spectrums. Figure 8 shows the variation of the normalized electric field (E_z) along with the surface current density (design 2) for the multiple values of the μ_c and frequency. Different resonating points have different changes in electric field intensity concertation, as seen in Fig. 8. Amplitude variation in the different resonating conditions depends on the field concentration over the edges of the graphene pixel geometry. We can identify from the overall results that the variation in the
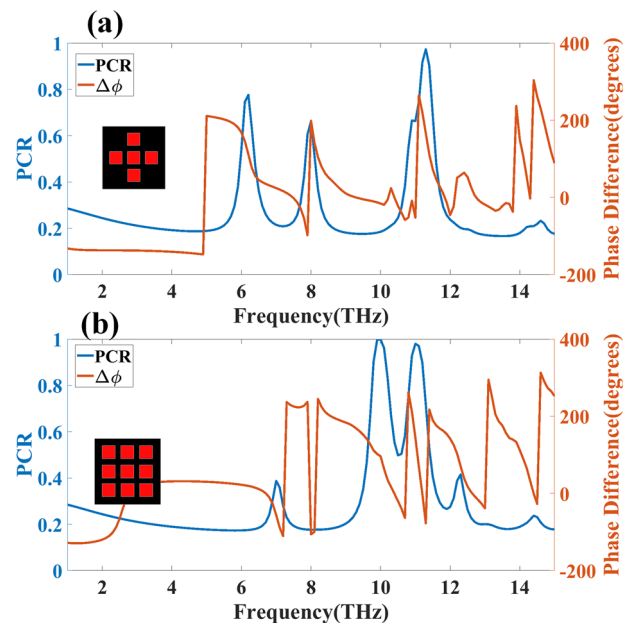

Fig. 6 Calculated variation in PCR for pixel, **a** design 1, **b** design 2

Fig. 7 Variation in PCR and phase difference for cross-polarization conditions for **a** design 1, **b** design 2 structure
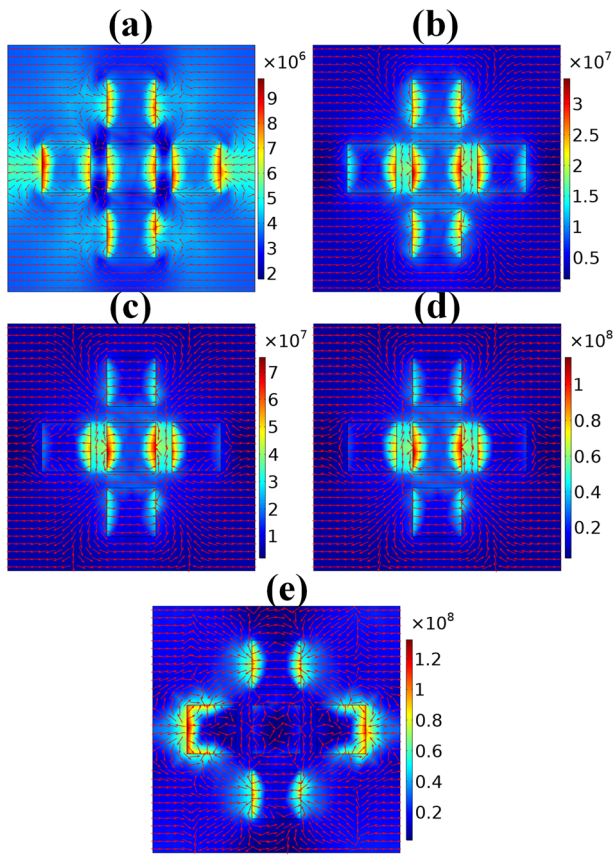
Fig. 8 Normalized electric field with surface current density for the design 2 array structure for **a** $\mu_c = 0.1$ eV and $\omega = 4$ THz, **b** $\mu_c = 0.3$ eV and $\omega = 3.6$ THz, **c** $\mu_c = 0.5$ eV and $\omega = 4.7$ THz, **d** $\mu_c = 0.7$ eV and $\omega = 5.5$ THz, **e** $\mu_c = 0.9$ eV and $\omega = 6.2$ THz

transmittance depends on the μ_c of the graphene. The pixel array of the graphene sheet is also responsible for the variation in various physical parameters such as phase difference,

PCR and transmittance. This variation allows us to choose the resonating band with suitable pixel array geometries and other physical parameters. We have compared the proposed pixel array-based polarizer structure with the other previously published results in terms of the dimensions, material used, broad-angle stability and types of graphene layers. This comparative analysis is shown in Table 1.

Various geometric factors and filed excitations can improve the performance of the PCR. As shown in Fig. 6, the PCR can be improvised by varying the graphene sheet's Fermi energy, which can be controlled by external voltage excitation. The pixel structure will be fixed in the case of Fermi energy. The values of PCR can also be improved by changing the width between the two pixels. The overall electric field concentration and dipole moments depend on the pixel gap. The large electric field concentration results in the reflectance and transmittance, resulting in overall PCR calculations.

3 Conclusion

Graphene-silica composited pixel array-based tunable polarizer is numerically investigated, resulting in the 1–15 THz of the infrared frequency range. This polarizer can be tuned by the different graphene Fermi energies/chemical potential values, which are ultimately controlled externally. The reflectance and transmittance were also determined to evaluate the device's performance as a linear to circular/elliptical polarization. The proposed structure also presented the variation in transmittance response for the different pixel configuration designs to identify the overall resonating behavior. It is possible to use the proposed polarizer structure across a wide range of THz frequencies because of its large bandwidth. With a wide range of incident angles up to

Table 1 A comparison of previously published structure with proposed pixel array-based graphene structure

References	Unit cell dimensions (µm³)	Material used for polarizer	Graphene layers	Oblique angle stability	Operating frequency band (THz)
This work	(1.5, 7.6, 7.6)	G–S	SL	80°	1–15
[57]	(59, 120, 120)	G–Au	SL	NA	0.4–1
[58]	(36, 10, 10)	G	SL	NA	1.23–2.73
[59]	(26, 100, 100)	M	M	40°	0.76–1.48
[60]	(25, 70, 70)	TN	SL	45°	1.17–2.99
[61]	(25, 16, 16)	G–Au	SL	40°	0.6–2.6
[62]	(90, 200, 200)	M	SL	70°	1.6–5
[63]	(18, 32, 32)	G	SL	NA	2–4
[64]	(125, 105, 105)	M	ML	60°	0.7–2.5
[65]	(19, 15, 15)	G	ML	NA	1.65–4.35
[66]	(0.25, 4, 4)	G–S	SL	NA	1–4

G graphene, *S* silica, *M* metal, *Au* gold, *TN* titanium nitride, *ML* multi-layered graphene structure, *SL* single-layered graphene structure

80 degrees, transmittance behavior remains constant for the proposed polarizer structure. New tunable THz devices for photonics circuits operating at lower THz frequencies may be developed due to the findings presented in this publication. Furthermore, large THz integrated systems can benefit from a simple, compact, and customizable graphene-based polarizer structure.

Author contributions FAA has conceived the project, gathered all the supportive information and supervised the overall project. VS has designed the structure that generates the results. All have contributed equally to writing the manuscript.

Data availability Correspondence and requests for materials should be addressed to VS.

Declarations

Conflict of interest The authors declare that they have no conflict of interest.

References

1. H.-H. Hsiao, C.H. Chu, D.P. Tsai, Fundamentals and applications of metasurfaces. Small Methods **1**(4), 1600064 (2017). https://doi.org/10.1002/smtd.201600064
2. S.B. Glybovski, S.A. Tretyakov, P.A. Belov, Y.S. Kivshar, C.R. Simovski, Metasurfaces: from microwaves to visible. Phys. Rep. **634**, 1–72 (2016). https://doi.org/10.1016/j.physrep.2016.04.004
3. A. Li, S. Singh, D. Sievenpiper, Metasurfaces and their applications. Nanophotonics **7**(6), 989–1011 (2018). https://doi.org/10.1515/nanoph-2017-0120
4. A.E. Minovich, A.E. Miroshnichenko, A.Y. Bykov, T.V. Murzina, D.N. Neshev, Y.S. Kivshar, Functional and nonlinear optical metasurfaces. Laser Photonics Rev. **9**(2), 195–213 (2015). https://doi.org/10.1002/lpor.201400402
5. V. Dave, V. Sorathiya, T. Guo, S.K. Patel, Graphene based tunable broadband far-infrared absorber. Superlatt. Microstruct. **124**, 113–120 (2018). https://doi.org/10.1016/j.spmi.2018.10.013
6. V. Sorathiya, V. Dave, Numerical study of a high negative refractive index based tunable metamaterial structure by graphene split ring resonator for far infrared frequency. Opt. Commun. **456**(June 2019), 124581 (2020). https://doi.org/10.1016/j.optcom.2019.124581
7. S.K. Patel, V. Sorathiya, S. Lavadiya, T.K. Nguyen, V. Dhasarathan, Polarization insensitive graphene-based tunable frequency selective surface for far-infrared frequency spectrum. Phys. E Low Dimensional Syst. Nanostruct. **120**, 114049 (2020). https://doi.org/10.1016/j.physe.2020.114049
8. A.K. Geim, K.S. Novoselov, The rise of graphene. Nat. Mater. **6**(3), 183–191 (2007). https://doi.org/10.1038/nmat1849
9. M. Bruna, S. Borini, Optical constants of graphene layers in the visible range. Appl. Phys. Lett. **94**(3), 1–4 (2009). https://doi.org/10.1063/1.3073717
10. L. Ju et al., Graphene plasmonics for tunable terahertz metamaterials. Nat. Nanotechnol. **6**(10), 630–634 (2011). https://doi.org/10.1038/nnano.2011.146
11. J. Xu, Z. Huang, B. Wu, X. Wu, Achieving perfect absorption of graphene in the near-infrared and visible wavelength ranges by critical coupling with a photonic crystal slab. 2016 Prog. Electromagn. Res. Symp. (2016). https://doi.org/10.1109/piers.2016.7735055
12. V.G. Veselago, The electrodynamics of substances with simultaneously negative values of ϵ and μ. Sov. Phys. Uspekhi **10**(4), 509–514 (1968). https://doi.org/10.1070/PU1968v010n04ABEH003699
13. J.B. Pendry, Negative refraction makes a perfect lens. Phys. Rev. Lett. **85**(18), 3966–3969 (2000). https://doi.org/10.1103/PhysRevLett.85.3966
14. S.K. Patel, V. Sorathiya, S. Lavadiya, L. Thomas, T.K. Nguyen, V. Dhasarathan, Multi-layered graphene silica-based tunable absorber for infrared wavelength based on circuit theory approach. Plasmonics **15**(6), 1767–1779 (2020). https://doi.org/10.1007/s11468-020-01191-x
15. J. Yao et al., Polarization dependence of optical pump-induced change of graphene extinction coefficient. Opt. Mater. Express **5**(7), 1341–1349 (2015). https://doi.org/10.1364/OME.5.001550
16. H. Liu, Y. Liu, D. Zhu, Chemical doping of graphene. J. Mater. Chem. **21**(10), 3335–3345 (2011). https://doi.org/10.1039/c0jm02922j
17. S.K. Patel, V. Sorathiya, Z. Sbeah, S. Lavadiya, T.K. Nguyen, V. Dhasarathan, Graphene-based tunable infrared multi band absorber. Opt. Commun. **474**, 126109 (2020). https://doi.org/10.1016/j.optcom.2020.126109
18. H. Zhang et al., Graphene-based fiber polarizer with PVB-enhanced light interaction. J. Light. Technol. **34**(15), 3563–3567 (2016). https://doi.org/10.1109/JLT.2016.2581315
19. X. Li, L. Lin, L.S. Wu, W.Y. Yin, J.F. Mao, A bandpass graphene frequency selective surface with tunable polarization rotation for THz applications. IEEE Trans. Antennas Propag. **65**(2), 662–672 (2017). https://doi.org/10.1109/TAP.2016.2633163
20. X. Huang, Z. Hu, P. Liu, Graphene based tunable fractal Hilbert curve array broadband radar absorbing screen for radar cross section reduction. AIP Adv. **4**(11), 117103 (2014). https://doi.org/10.1063/1.4901187
21. S. Liu et al., Anisotropic coding metamaterials and their powerful manipulation of differently polarized terahertz waves. Light Sci. Appl. **5**(5), e16076 (2016). https://doi.org/10.1038/lsa.2016.76
22. A. Pandya, V. Sorathiya, S. Lavadiya, Graphene-based nanophotonic devices, in *Recent Advances in Nanophotonics—Fundamentals and Applications*. IntechOpen (2020). https://doi.org/10.5772/intechopen.93853
23. B. Wu, Y.J. Yang, H.L. Li, Y.T. Zhao, C. Fan, W.B. Lu, Low-loss dual-polarized frequency-selective rasorber with graphene-based planar resistor. IEEE Trans. Antennas Propag. **68**(11), 7439–7446 (2020). https://doi.org/10.1109/TAP.2020.2998173
24. L. Qi, C. Liu, Broadband multilayer graphene metamaterial absorbers. Opt. Mater. Express **9**(3), 1298 (2019). https://doi.org/10.1364/ome.9.001298
25. V. Sorathiya, S.K. Patel, D. Katrodiya, Tunable graphene-silica hybrid metasurface for far-infrared frequency. Opt. Mater. (Amst.) **91**, 155–170 (2019). https://doi.org/10.1016/j.optmat.2019.02.053
26. Z. Song, K. Wang, J. Li, Q.H. Liu, Broadband tunable terahertz absorber based on vanadium dioxide metamaterials. Opt. Express **26**(6), 7148 (2018). https://doi.org/10.1364/OE.26.007148
27. D.R. Smith, W.J. Padilla, D.C. Vier, S.C. Nemat-Nasser, S. Schultz, Composite medium with simultaneously negative

permeability and permittivity. Phys. Rev. Lett. **84**(18), 4184–4187 (2000). https://doi.org/10.1103/PhysRevLett.84.4184

28. G.W. Hanson, Dyadic green's functions for an anisotropic, non-local model of biased graphene. IEEE Trans. Antennas Propag. **56**(3), 747–757 (2008). https://doi.org/10.1109/TAP.2008.917005

29. H. Xiong, Y.-B. Wu, J. Dong, M.-C. Tang, Y.-N. Jiang, X.-P. Zeng, Ultra-thin and broadband tunable metamaterial graphene absorber. Opt. Express **26**(2), 1681 (2018). https://doi.org/10.1364/OE.26.001681

30. T. Stauber, N.M.R. Peres, A.K. Geim, Optical conductivity of graphene in the visible region of the spectrum. Phys. Rev. B Condens. Matter Mater. Phys. **78**(8), 1–8 (2008). https://doi.org/10.1103/PhysRevB.78.085432

31. G.W. Hanson, Dyadic Green's functions and guided surface waves for a surface conductivity model of graphene. J. Appl. Phys. (2008). https://doi.org/10.1063/1.2891452

32. J. Horng et al., Drude conductivity of Dirac fermions in graphene. Phys. Rev. B Condens. Matter Mater. Phys. **83**(16), 165113 (2011). https://doi.org/10.1103/PhysRevB.83.165113

33. Z.Q. Li et al., Dirac charge dynamics in graphene by infrared spectroscopy. Nat. Phys. **4**(7), 532–535 (2008). https://doi.org/10.1038/nphys989

34. R. Panwar, J.R. Lee, Progress in frequency selective surface-based smart electromagnetic structures: a critical review. Aerosp. Sci. Technol. **66**, 216–234 (2017). https://doi.org/10.1016/j.ast.2017.03.006

35. R. Mishra, A. Sahu, R. Panwar, Cascaded graphene frequency selective surface integrated tunable broadband terahertz metamaterial absorber. IEEE Photonics J. (2019). https://doi.org/10.1109/JPHOT.2019.2900402

36. N. Liu, X. Sheng, C. Zhang, D. Guo, Design of frequency selective surface structure with high angular stability for radome application. IEEE Antennas Wirel. Propag. Lett. **17**(1), 138–141 (2018). https://doi.org/10.1109/LAWP.2017.2778078

37. Q. Zhou et al., Independently controllable dual-band terahertz metamaterial absorber exploiting graphene. J. Phys. D. Appl. Phys. (2019). https://doi.org/10.1088/1361-6463/ab132a

38. H. Huang, H. Xia, W. Xie, Z. Guo, H. Li, D. Xie, Design of broadband graphene-metamaterial absorbers for permittivity sensing at mid-infrared regions. Sci. Rep. **8**(1), 4183 (2018). https://doi.org/10.1038/s41598-018-22536-x

39. H. Lin et al., A 90-nm-thick graphene metamaterial for strong and extremely broadband absorption of unpolarized light. Nat. Photonics **13**(4), 270–276 (2019). https://doi.org/10.1038/s41566-019-0389-3

40. T. Guo, C. Argyropoulos, Broadband polarizers based on graphene metasurfaces. Opt. Lett. **41**(23), 5592 (2016). https://doi.org/10.1364/OL.41.005592

41. Y. Niu, J. Wang, Z. Hu, F. Zhang, Tunable plasmon-induced transparency with graphene-based *T*-shaped array metasurfaces. Opt. Commun. **416**(January), 77–83 (2018). https://doi.org/10.1016/j.optcom.2018.02.009

42. B. Jin, T. Guo, C. Argyropoulos, Enhanced third harmonic generation with graphene metasurfaces. J. Opt. (UK) (2017). https://doi.org/10.1088/2040-8986/aa8280

43. K. Meng et al., Tunable broadband terahertz polarizer using graphene-metal hybrid metasurface. Opt. Express **27**(23), 33768 (2019). https://doi.org/10.1364/OE.27.033768

44. H. Li, Y. Zhang, H. Xiao, M. Qin, S. Xia, L. Wang, Investigation of acoustic plasmons in vertically stacked metal/dielectric/graphene heterostructures for multiband coherent perfect absorption. Opt. Express **28**(25), 37577 (2020). https://doi.org/10.1364/oe.411795

45. H. Li, C. Ji, Y. Ren, J. Hu, M. Qin, L. Wang, Investigation of multiband plasmonic metamaterial perfect absorbers based on graphene ribbons by the phase-coupled method. Carbon N. Y.

141, 481–487 (2019). https://doi.org/10.1016/j.carbon.2018.10.002

46. N. Petrone et al., Chemical vapor deposition-derived graphene with electrical performance of exfoliated graphene. Nano Lett. **12**(6), 2751–2756 (2012). https://doi.org/10.1021/nl204481s

47. E. Moreau et al., Graphene growth by molecular beam epitaxy on the carbon-face of SiC. Appl. Phys. Lett. **97**(24), 241907 (2010). https://doi.org/10.1063/1.3526720

48. K.S. Novoselov et al., Two-dimensional atomic crystals. Proc. Natl. Acad. Sci. USA **102**(30), 10451–10453 (2005). https://doi.org/10.1073/pnas.0502848102

49. L. Song, L. Ci, W. Gao, P.M. Ajayan, Transfer printing of graphene using gold film. ACS Nano **3**(6), 1353–1356 (2009). https://doi.org/10.1021/nn9003082

50. T. Zou et al., High-speed femtosecond laser plasmonic lithography and reduction of graphene oxide for anisotropic photoresponse. Light Sci. Appl. (2020). https://doi.org/10.1038/s41377-020-0311-2

51. M.C. Sherrott et al., Experimental demonstration of > 230° phase modulation in gate-tunable graphene-gold reconfigurable mid-infrared metasurfaces. Nano Lett. **17**(5), 3027–3034 (2017). https://doi.org/10.1021/acs.nanolett.7b00359

52. G.B. Barin, Y. Song, I.D.F. Gimenez, A.G.S. Filho, L.S. Barreto, J. Kong, Optimized graphene transfer: influence of polymethylmethacrylate (PMMA) layer concentration and baking time on grapheme final performance. Carbon N. Y. **84**(C), 82–90 (2015). https://doi.org/10.1016/j.carbon.2014.11.040

53. M.P. Lavin-Lopez, J.L. Valverde, A. Garrido, L. Sanchez-Silva, P. Martinez, A. Romero-Izquierdo, Novel etchings to transfer CVD-grown graphene from copper to arbitrary substrates. Chem. Phys. Lett. **614**, 89–94 (2014). https://doi.org/10.1016/j.cplett.2014.09.019

54. B.J. Kim, H. Jang, S.K. Lee, B.H. Hong, J.H. Ahn, J.H. Cho, High-performance flexible graphene field effect transistors with ion gel gate dielectrics. Nano Lett. **10**(9), 3464–3466 (2010). https://doi.org/10.1021/nl101559n

55. Z. Miao et al., Widely tunable terahertz phase modulation with gate-controlled graphene metasurfaces. Phys. Rev. X **5**(4), 41027 (2015). https://doi.org/10.1103/PhysRevX.5.041027

56. J. Ding et al., Mid-infrared tunable dual-frequency cross polarization converters using graphene-based *L*-shaped nanoslot array. Plasmonics **10**(2), 351–356 (2015). https://doi.org/10.1007/s11468-014-9816-y

57. X. Yu, X. Gao, W. Qiao, L. Wen, W. Yang, Broadband tunable polarization converter realized by graphene-based metamaterial. IEEE Photonics Technol. Lett. **28**(21), 2399–2402 (2016). https://doi.org/10.1109/LPT.2016.2596843

58. Z. Hu, M. Aqeeli, X. Zhang, X. Huang, A. Alburaikan, Design of broadband and tunable terahertz absorbers based on graphene metasurface: equivalent circuit model approach. IET Microw. Antennas Propag. **9**(4), 307–312 (2015). https://doi.org/10.1049/iet-map.2014.0152

59. S. Liu, H. Chen, T.J. Cui, A broadband terahertz absorber using multi-layer stacked bars. Appl. Phys. Lett. **106**(15), 1–6 (2015). https://doi.org/10.1063/1.4918289

60. G. Deng, J. Yang, Z. Yin, Broadband terahertz metamaterial absorber based on tantalum nitride. Appl. Opt. **56**(9), 2449 (2017). https://doi.org/10.1364/ao.56.002449

61. J. Zhu, S. Li, L. Deng, C. Zhang, Y. Yang, H. Zhu, Broadband tunable terahertz polarization converter based on a sinusoidally-slotted graphene metamaterial. Opt. Mater. Express **8**(5), 1164 (2018). https://doi.org/10.1364/OME.8.001164

62. X. Liu, Q. Zhang, X. Cui, Ultra-broadband polarization-independent wide-angle THz absorber based on plasmonic resonances in semiconductor square nut-shaped metamaterials.

Plasmonics **12**(4), 1137–1144 (2017). https://doi.org/10.1007/s11468-016-0368-1

63. E.S. Torabi, A. Fallahi, A. Yahaghi, Evolutionary optimization of graphene-metal metasurfaces for tunable broadband terahertz absorption. IEEE Trans. Antennas Propag. **65**(3), 1464–1467 (2017). https://doi.org/10.1109/TAP.2016.2647580

64. C. Shi et al., Compact broadband terahertz perfect absorber based on multi-interference and diffraction effects. IEEE Trans. Terahertz Sci. Technol. **6**(1), 40–44 (2016). https://doi.org/10.1109/TTHZ.2015.2496313

65. A. Fardoost, F.G. Vanani, A. Amirhosseini, R. Safian, Design of a multilayer graphene-based ultrawideband terahertz absorber. IEEE Trans. Nanotechnol. **16**(1), 68–74 (2017). https://doi.org/10.1109/TNANO.2016.2627939

66. E. Gao et al., Dynamically tunable dual plasmon-induced transparency and absorption based on a single-layer patterned graphene metamaterial. Opt. Express **27**(10), 13884 (2019). https://doi.org/10.1364/oe.27.013884